Failure Analysis of Bamboo Bolt Connection in Uniaxial Tension by FEM by Considering Fiber Direction

Raviduth Ramful

Abstract

Full-culm bamboo has been used for millennia in construction. Specific connections are normally required to suit its unique morphology and nonuniform structure. Presently, the use of full-culm bamboo is limited in the construction industry as a result of a lack of information and test standards about the use and evaluation of full-culm connections. This study aims to further explore this area by investigating the failure modes in bamboo bolt connections in uniaxial tension by considering fiber direction in finite element analysis. Three types of bolt configurations of varying permutations, namely, single, dual, and orthogonal, were investigated. An orthotropic material was used as a constitutive model in finite element formulation to capture the inhomogeneity prevailing in bamboo culm. From the strain-field analysis of a hollow-inhomogeneous model representing bamboo, shear-out failure was dominant, as a localized area equivalent to the bolt diameter was affected due to high material orthotropy with high axial strength but weak radial and tangential strength. Bearing failure is assumed to precede shear-out failure at the bolt–bamboo contact interface, as the embedding strength was affected by localized strain concentration. The strain distribution in various bolt arrangements was found to vary between bolted connections of inhomogeneous-hollow geometry of bamboo and the ones of inhomogeneous-solid geometry representing timber. The observation in this study highlights the need for alternative design criteria to specifically assess the damage mechanism in bamboo connections.

As one of the oldest construction materials, bamboo has been widely used as a reliable structural material in rural houses and bridges in several Asian and Latin American countries in the past millennia. It has attracted much attention in recent years because of its distinctive sustainability attributes and excellent mechanical characteristics. Unlike timber, bamboo has a fast growth rate, and those with optimum strength can be harvested after reaching maturity in 3 to 4 years (Liese 1987). In terms of mechanical strength, it outperforms timber based on its high strength-to-weight ratio (Ashby et al. 1995). Even so, its unlimited use in the construction industry is hindered because of natural variation in its morphology and by a lack of standards and building codes, hence restricting its use to basic structures (Gatoo et al. 2014). One area with a notable shortfall of applicable standards is for bamboo connections. To maximize the use of bamboo in building construction, specific connection types are normally required as a result of its inherent structural nonuniformity and unique morphology comprised of a round, hollow, and tapered structure (Correal 2016).

Several types of bamboo connections, ranging from traditional to modern types, have been developed with varying load-carrying capacity. Their efficacy rests on the types of fasteners used and the orientation of joined members (Correal 2016, Hong et al. 2019). Janssen (2000) has proposed three criteria for the classification of joints: (1) joints involving contact between full cross sections or connected via joining elements linked to cross sections, (2) collecting forces within the hollow section or from the outside of the culm, and (3) the alignment of the joining element with respect to fiber direction. In addition, the strength and efficacy of the joint is specifically affected by the type of connector, the end shape of the bamboo culms, and the internode filling material (Janssen 2000). The dowel connection, which uses a steel bolt as a connector, is one of the most widely used connections in bamboo given its simplicity and reliability. The load capacity of the dowel-type connection is influenced by several factors, namely, bolt diameter, bolt strength, bamboo diameter, direction of loading, and moisture content, among others (Li et al. 2020, Sotayo et al. 2020, Wang and Yang 2020). It has been found that the direction of loading parallel to main and side

The author is at Kyoto Institute of Technology, Kyoto, Japan (r.ramful@uom.ac.mu [corresponding author]). This paper was received for publication in October 2020. Article no. 20-00066.

Forest Prod. J. 71(1):58–64.
doi:10.13073/FPJ-D-20-00066

bamboo culms yielded the best results in comparison to perpendicular loading members. In addition, the compressive strength parallel to grain was found to decrease with increasing moisture content as observed in other cellulose-reinforced composite material similar to bamboo (Yang et al. 2020). In general, bamboo tends to behave nonlinearly in conditions of excessive humidity above 60 percent and linearly in conditions of humidity below 40 percent (Askarinejad et al. 2015). Additionally, the variation in culm morphology, such as tapered geometry and fiber density, which increases with height, also influences the strength of the culm connection (Correal 2016).

Failure of bamboo connections can occur in many ways, namely, due to material failure as a result of its inherent inhomogeneity or failure in the joining element. Full-culm bamboo in the external loading mode exhibits a complex deformation behavior as a result of its high anisotropy (Kappel et al. 2004, Spatz and Niklas 2013, Askarinejad et al. 2015, Deng et al. 2016, Huang et al. 2017, Trujillo et al. 2017, Zhang et al. 2017, Gauss et al. 2019). In previous studies, four types of prevalent modes of failure have been reported in timber and laminated wood and bamboo products involving bolted connections (Hong et al. 2020). These are bearing, net tension, shear-out, and cleavage (Coelho and Mottram 2015). In bearing failure, the contact area at the hole edge is affected and is expected to occur in a high width-to-hole diameter component, while in net-tension failure, sudden cracks orthogonal to the direction of loading propagate due to a small cross-sectional area. Shear-out failure occurs in bolt arrangements with short end distances and is characterized by shear stresses that occur along the shear-out planes, while cleavage failure occurs as the result of a combination of the latter and net-tension failure. Previous studies on failure analysis of bolted connections in axial tension in full-culm and laminated bamboo have resulted in longitudinal shear plug formation (Reynolds et al. 2016, Ramful 2018). However, as stated by Reynolds et al. (2016), conventional design rules and practices used to prevent split in timber products are not applicable to bamboo, as it exhibits different failure modes. The progressive deformation consisting of localized buckling of fibers and crushing of matrix in bearing failure is characterized by embedding strength (Olmedo and Santiuste 2012, Coelho and Mottram 2015, Hong et al. 2020). In bamboo laminates, the embedding strength parallel to grain exceeds that of perpendicular to grain (Sawata and Yasumura 2002, Eratodi et al. 2012). In addition, the embedding strength in bamboo laminates perpendicular to grain was found to further decrease with increasing bolt diameter (Zhou et al. 2018).

From previous studies, connections in bamboo laminates were found to be affected by several influential factors, namely, diameter of connectors, laminate thickness, direction of loading, and embedding strength (Cui et al. 2020, Hu and Zhang 2020). Even though the weaknesses of full-culm bamboo is well described in literature, the outcome due to its inhomogeneous material characteristics and unique geometry on mechanical performance of connections is limited. The lack of information on the full-culm connection is demonstrated by a lack of standards and building codes in this area, restricting its use in complex and modern construction. To overcome the material constraints in bamboo culms, the finite element method (FEM) has been widely used to investigate its material limitation and failure modes (Askarinejad et al. 2015, Keogh et al. 2015, Paraskeva et al. 2017). This study aims to address this gap by investigating the failure modes of bamboo bolt connections in uniaxial tension by considering fiber direction in FEM.

Finite Element Analysis of the Bamboo Connection

In this section, the bamboo–bolt connection was simulated in implicit mode in uniaxial tension in the commercial FEM software LS-DYNA (version 4.3; Livermore Software Technology, USA). The results of the hollow-inhomogeneous model of bamboo was compared with the solid-inhomogeneous model representing timber and with other models of homogeneous material characteristics.

Material properties and models

The homogeneous material in this study was based on a simple isotropic model assigned with engineering constants of an elastic material, as displayed in Table 1. From previous experimental investigation (Ramful et al. 2020), an average modulus of elasticity, E, of 15 GPa was obtained, while the Poisson ratio, v, was determined from past literature data as 0.3 (Keogh et al. 2015). The engineering constants of an orthotropic material were used to simulate the inhomogeneous nature of bamboo, as displayed in Table 2. These values are estimates based on the optimized transverse isotropy of bamboo, which was assumed to have a longitudinal-to-transverse bending stiffness ratio of 100:4.5 (Ramful and Sakuma 2020). The bolt in this study was assumed as a rigid section such that it will not undergo any deformation. The study focused mainly on the damage mechanisms within bamboo culm material. In the rigid material setting, it was assigned a Young's modulus value much greater than bamboo material. The rigid material setting was selected in order to apply constraints in the global direction. The displacement of the bolt was thus restricted only to the axial direction to simulate the connection in the uniaxial tension mode. The material density was taken as 700 kg/m^3 (Trujillo and Lopez 2016).

Table 1.—Homogeneous material (isotropic model) parameters used in the finite element method.

Parameter	Value
Elastic modulus (MPa), E	15,000
Poisson ratio, v	0.3

Table 2.—Inhomogeneous material (orthotropic model) parameters used in the finite element method.

Parameter	Value
Elastic modulus (MPa)	
E_L	15,000
E_T	675
Poisson ratio	
v_L	0.3
v_T	0.0135
Shear modulus (MPa)	
G_L	630

Geometrical modeling and boundary conditions

Three types of bolt configurations of varying permutation, namely, single, dual, and orthogonal, were selected in this study, as shown in Figure 1. One full solid cylindrical internode section was considered in this study, and the physical model was constructed based on morphological data of Madake bamboo (*Phyllostachys bambusoides*). The outer diameter, wall thickness, and intermodal length were taken as 100, 12, and 450 mm, respectively, for an internode count of 18 (Ghavami 2016). The bolt diameter, ϕ_B, was 9 mm with a clearance of 0.5 mm with the hole wall section. A displacement of 1 mm/min was applied to the rigid bolt by prescribed motion, as illustrated in Figure 1d. At the wall end, movement was restricted in the x, y, and z directions.

According to the Eurocode 5 standard, the embedding strength is calculated from the bolt diameter and the density as follows:

$$fe_\alpha = \frac{0.082(1 - 0.01d)\rho}{k_{90}\sin^2\alpha + \cos^2\alpha} \quad (1)$$

where

$$k_{90} = \begin{cases} 1.35 + 0.015d & \text{for softwoods} \\ 1.30 + 0.015d & \text{for laminates} \\ 0.90 + 0.015d & \text{for hardwoods} \end{cases} \quad (2)$$

and fe_α is the embedding strength in MPa, k_{90} is the material constant when loaded perpendicular to grain, d is the bolt diameter in mm, ρ is the density in kg/m^3, and α is the loading angle to grain direction (EN 1995-1-1 2004). In this study, the parameters d, ρ, and α were kept constant to minimize variability in strain field analysis in order to discern principal changes in terms of damage mechanisms and embedding strength due to the effect of geometry and the material model.

FE mesh

The 3D model was designed and meshed on FEMAP (version 12.0.1a; Siemens Digital Industries Software, USA), a finite element model–building software, and tetrahedral mesh solid was applied, with finer mesh at the bolt-bamboo connection, as shown in Figure 2a.

Results and Discussion

Strain field analysis

The strain field results of various geometry-material models of three-bolt configurations in uniaxial tension are displayed in Figures 3 through 5. The observed variation in the strain field occurred as a result of change in material property, geometry, and bolt configurations. In this analysis, the applied displacement was resisted mainly by embedding strength in the surrounding material rather than shear in the connector, as the rigid bolt was considered.

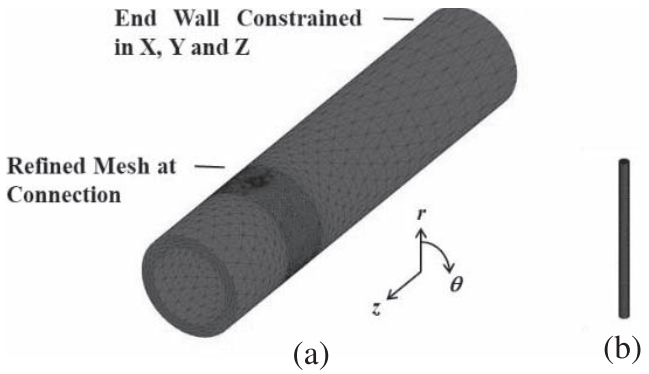

Figure 2.—Tetrahedral mesh solid of (a) bamboo model in single-bolt configuration (no. of elements: 93,929, no. of nodes: 142,649); (b) bolt model (no. of elements: 64,385, no. of nodes: 11,624).

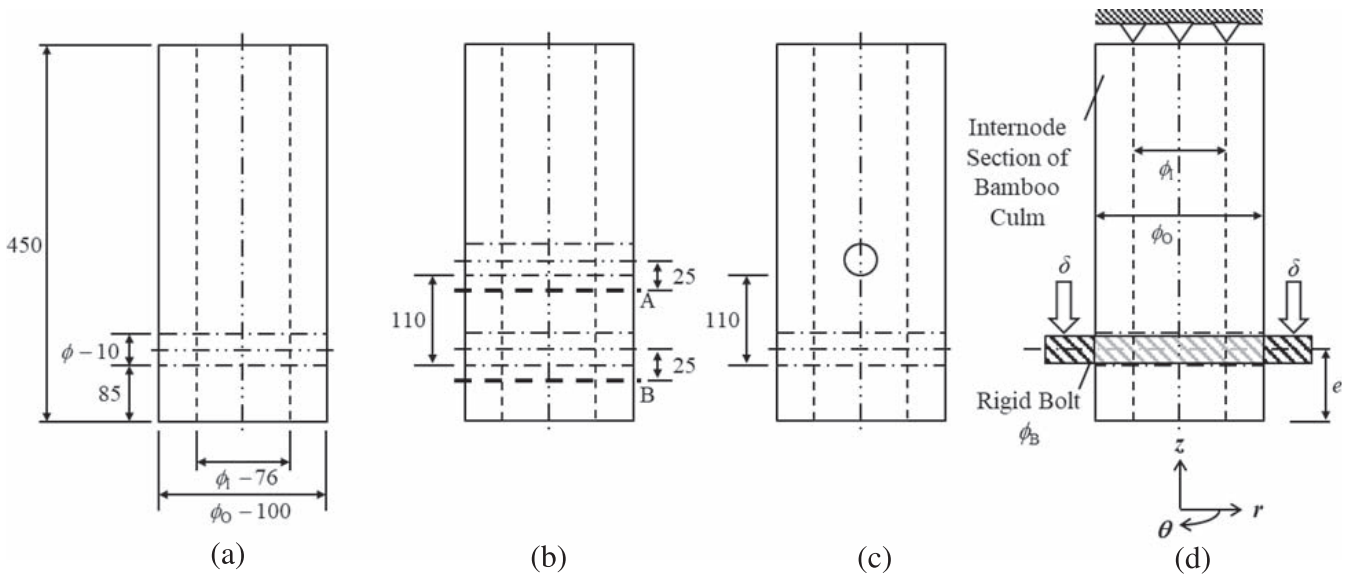

Figure 1.—Schematic illustration of bolted connections evaluated: (a) single configuration, (b) dual configuration, (c) orthogonal configuration; and (d) boundary condition in axial tension mode setup.

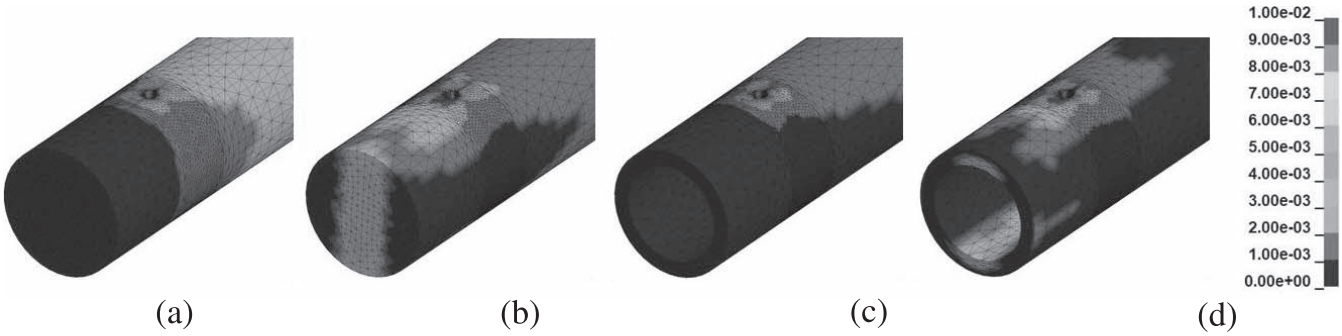

Figure 3.—Fringe plots of maximum principal strain of (a) solid-homogeneous, (b) solid-inhomogeneous, (c) hollow-homogeneous, and (d) hollow-inhomogeneous models in single-bolt configuration.

Damage mechanisms

The main failure modes in the four types of geometry-material models of single-bolted connections due to axial tension are depicted in Figure 6. These were shear-out failure and net-tension failure. These failure modes observed in the four types of geometry-material models were recurrent in all three types of bolt configuration regardless of bolt permutations. In each failure mode, the effect due to homogeneous and inhomogeneous material characteristics can be easily distinguished from the side-by-side comparison. The effect of short-end distance on shear-out failure in this study was negligible, as the ratio of end distance to diameter, e/ϕ_B, was greater than 4 (Coelho and Mottram 2015). Shear-out failure, which occurred mainly in solid-inhomogeneous and hollow-inhomogeneous models, affected a localized area equivalent to the bolt diameter, as shown in Figures 6a and 6c. This phenomenon, which occurred in inhomogeneous material, can be explained by the high orthotropicity resulting in high strength axially but weak strength radially and tangentially.

In addition to shear-out failure in solid-inhomogeneous and hollow-inhomogeneous models, bearing failure is anticipated to occur at the bolt-member contact interface due to the effect of embedding strength. This is demonstrated by the region of strain concentration in the fringe plots of Figures 3b, 3d, 4b, 4d, 5b, and 5d. The progressive deformation associated with bearing failure due to the localized buckling of fibers and the crushing of matrix increases the deformation capacity of the connection (Olmedo and Santiuste 2012). This mode of failure is assumed to provide damage-tolerant bolted connections rather than brittle shear-out or net-tension failure modes (Coelho and Mottram 2015).

Net-tension failure occurred mainly in solid-homogeneous and hollow-homogeneous models, whereby the axial tensile forces exerted by the bolt uniformly affected the whole cross-sectional area, as shown in Figures 6b and 6d. Net-tension failure, which affected mainly homogeneous material, can be explained by the uniform load distribution across its cross section due to material uniformity. In net-tension failure, instantaneous cracks propagated in a direction transverse to that of axial loading and is assumed to be influenced by the cross-sectional area of the main member. From Figures 4a, 4c, 5a, and 5c, net-tension failure was found to be dominant in multirow bolted connections. This observation corresponds to previous reports that attributed this failure to high stress concentration originating from specific rows in successive arrangements (Mottram and Turvey 1998).

Analysis of strain distribution

The deformation due to bolt arrangements in various geometry-material models is quantitatively discussed by analyzing the maximum principal strain distribution in the periphery of the bolt-member contact interface. Figure 7 shows the distribution of maximum principal strain in terms of azimuthal angle, θ, along the transverse sliced sections A and B located at a distance of 25 mm from the bolt axis, as indicated in Figure 1b. The azimuthal angle is interpreted clockwise from the radial axis.

The distinct peaks at azimuthal angles 0°, 180°, 90°, and 270° (Figs. 7a, 7c–7f) in solid-inhomogeneous and hollow-

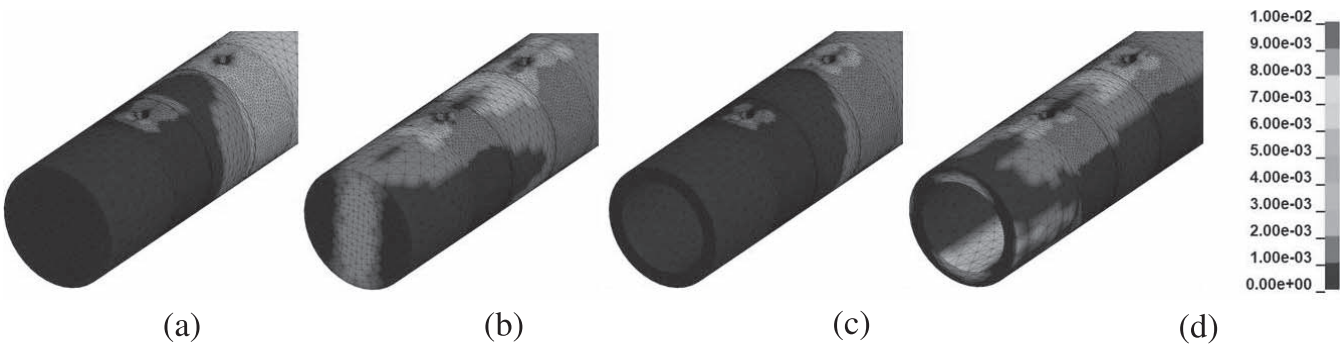

Figure 4.—Fringe plots of maximum principal strain of (a) solid-homogeneous, (b) solid-inhomogeneous, (c) hollow-homogeneous, and (d) hollow-inhomogeneous models in dual-bolt configuration.

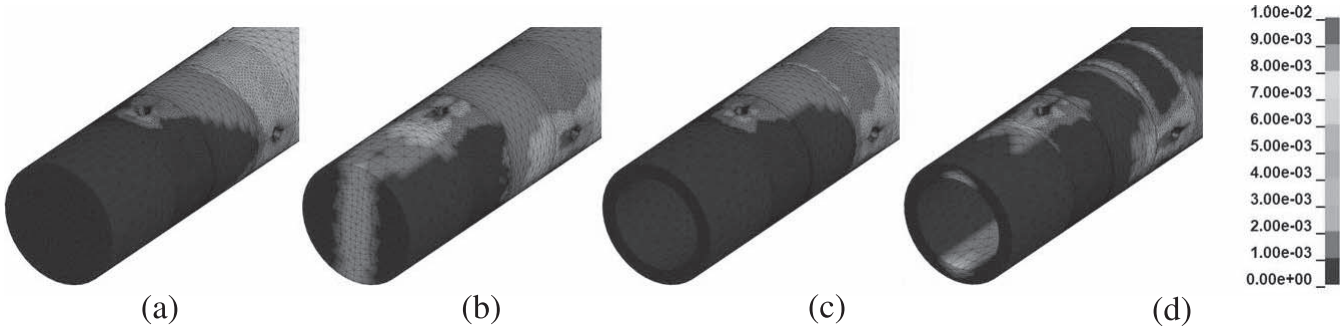

Figure 5.—Fringe plots of maximum principal strain of (a) solid-homogeneous, (b) solid-inhomogeneous, (c) hollow-homogeneous, and (d) hollow-inhomogeneous models in orthogonal bolt configuration.

inhomogeneous models demonstrate a narrowed region of strain concentration that is in line with the previous observation made about shear-out failure. This localized increase is assumed to further affect the embedding strength, leading to bearing failure. Furthermore, in dual configurations involving same geometry-material models, the strain distribution in the periphery of the first row was altered (Fig. 7c). The compressive effect induced by the second row restrained the full tensile effect on the first row, hence the reduction in strain as observed by the difference between Figures 7c and 7a. Conversely, the constant strain distribution around azimuthal angle θ in solid-homogeneous and hollow-homogeneous models (Figs. 7a, 7c–7f) confirmed the net-tension failure as previously discussed.

The normalized values of the first row, based on corresponding maximum principal strain (6.33×10^{-3}) obtained from the solid-inhomogeneous model in the single-bolt configuration, are shown in Table 3. The maximum principal strain distribution in inhomogeneous material models noticeably exceeded homogeneous ones and was specifically greater in solid as compared to hollow geometries. This difference between bolted connections of the inhomogeneous-hollow model of bamboo and the inhomogeneous-solid model representing timber is further pronounced in the second-row arrangement (Figs. 7d and 7f).

In a previous study, the failure observed in bamboo was reported to distinctly differ from solid wood structure with a higher ratio of wall thickness to radius. According to Huang et al. (2017), tubular plant materials inherit a high strength-to-weight ratio and low weight per unit length, enabling them to better resist deformation in various modes of loading in comparison to solid cylindrical materials of the same weight.

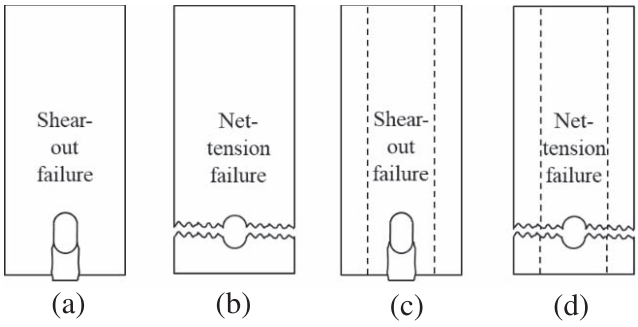

Figure 6.—Schematic illustration of damage mechanisms in (a) solid-inhomogeneous, (b) solid homogeneous, (c) hollow-inhomogeneous, and (d) hollow-homogeneous models in single-bolt configuration.

Future recommendation

As per the normalized embedding strength results in Table 4 according to the Eurocode 5 standard, the embedding strength of the material increases with density and decreases with increasing bolt diameter as well as when loaded perpendicular to the grain direction. Eurocode 5 uses a standard expression to estimate the embedment strength parallel to grain direction in various wood-related materials based simply on density and bolt diameter (EN 1995-1-1 2004).

However, due to the lack of provision for bamboo material in common standards such as Eurocode 5, the embedment strength due to varying bolt diameter and changes in loading with respect to grain direction has to be further researched for precise results. This will add to the establishment of specific standards for bamboo connections.

Conclusion

In this study, the damage mechanisms of three types of bolt–bamboo connections were investigated in uniaxial tension by considering fiber direction. The following conclusions were made from the strain-field analysis of the hollow-inhomogeneous model representing bamboo:

1. Shear-out failure was dominant and affected a localized area equivalent to bolt diameter due to high material orthotropy, which provided high axial strength but weak radial and tangential strength.
2. In addition to shear-out failure, bearing failure was anticipated to occur at the bolt–bamboo contact interface as the embedding strength was affected by localized strain concentration. A high width-to-hole diameter in bamboo is likely to further accentuate bearing failure.

This study provided useful insights by highlighting the damage mechanisms that prevailed in bolted connections of inhomogeneous-hollow geometry of bamboo as compared to the ones of inhomogeneous-solid geometry representing timber.

The strain distribution observed in these two unique geometry-material models varied according to bolt arrangements, underlining the need of alternative design criteria to specifically assess the damage mechanism in bamboo connections.

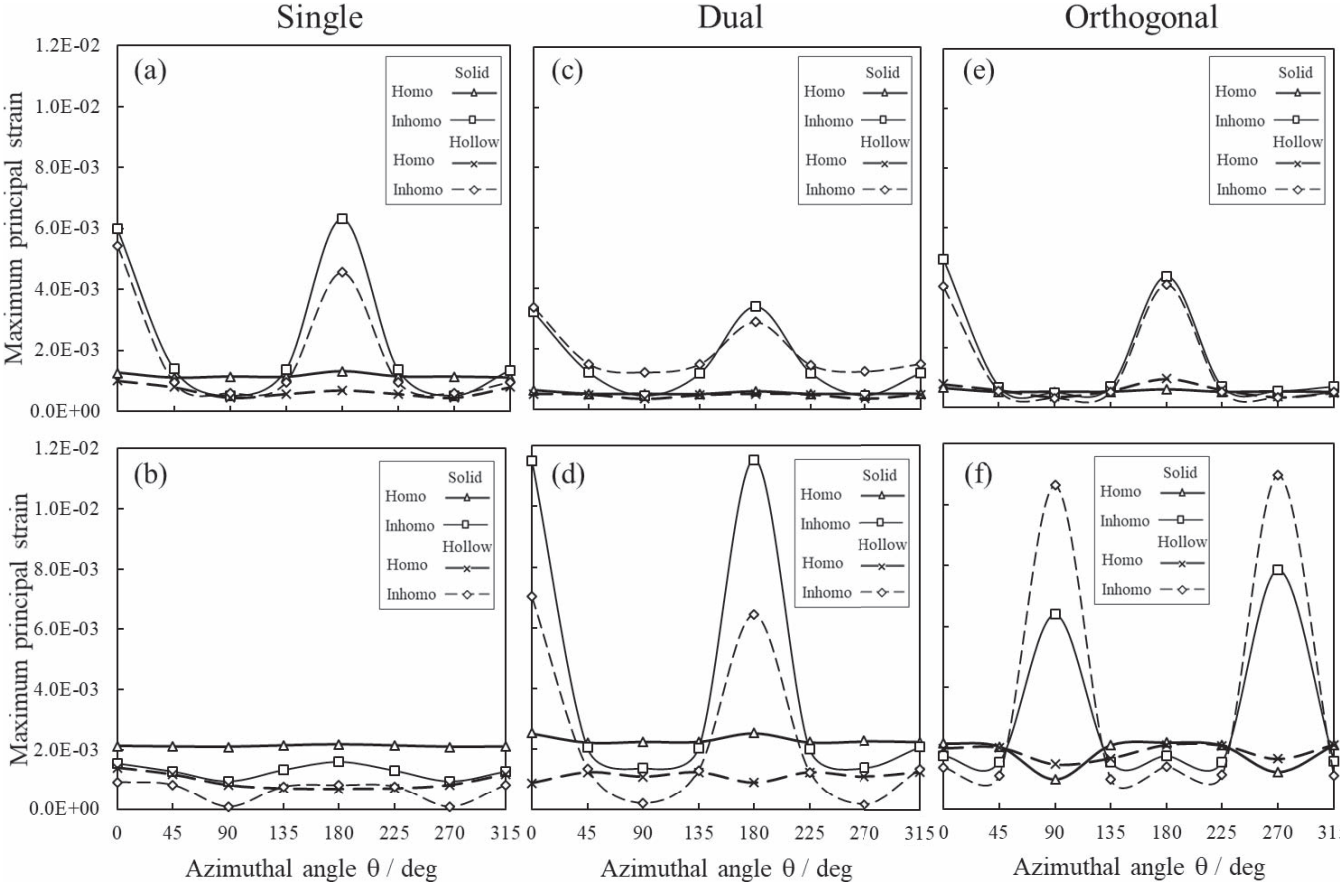

Figure 7.—Distribution of maximum principal strain in terms of azimuthal angle, θ, along the transverse sliced sections A and B in three-bolt configurations corresponding to (a), (c), and (e) first row, and (b), (d), and (f), second row.

Table 3.—Nondimensional values of maximum principal strain of foremost hole at circumferential angle of 0° and 180°.[a]

Model		Normalized maximum principal strain, ε_1, of first row (azimuthal angle 0°, 180°)		
Geometry model	Material model	Single	Dual	Orthogonal
Solid	Inhomogeneous	1.000	0.539	0.694
	Homogeneous	0.207	0.094	0.097
Hollow	Inhomogeneous	0.720	0.456	0.651
	Homogeneous	0.109	0.080	0.152

[a] All data are normalized by the greatest value of maximum principal strain (6.33×10^{-3}) obtained from the solid-inhomogeneous model.

Table 4.—Nondimensional values of embedding strength based on the Eurocode 5 standard.[a]

		Normalized characteristic embedment strength (N/mm^2)			
		$d = 9$ mm		$d = 18$ mm	
		Angle α of the load to the grain (°)			
Material type	Density (kg/m^3)	0	90	0	90
Softwood	400	0.500	0.335	0.451	0.278
Bamboo	700	0.875	0.610	0.788	0.502
Hardwood	800	1.000	0.966	0.901	0.770

[a] All data are normalized by the greatest value of embedding strength (60 N/mm^2) obtained from hardwood connections involving 9-mm bolt diameter and loaded parallel to grain direction.

Further research in terms of numerical investigation supported by experimental results is required to establish relevant standards in bamboo building construction, as this study was limited to specific geometry and a unique mode of loading.

Literature Cited

Ashby, M. F., L. J. Gibson, U. Wegst, and R. Olive. 1995. The mechanical properties of natural materials. I. Material property charts. *Proc. R. Soc. Lond. A* 450:123–140.

Askarinejad, S., P. Kotowski, F. Shalchy, and N. Rahbar. 2015. Effects of humidity on shear behavior of bamboo. *Theor. Appl. Mech. Lett*. 5:236–243.

Coelho, A. M. G. and J. T. Mottram. 2015. A review of the behaviour and analysis of bolted connections and joints in pultruded fibre reinforced polymers. *Mater. Des*. 74:86–107.

Correal, J. F. 2016. Bamboo design and construction. *In:* Nonconventional and Vernacular Construction Materials. K. A. Harries and B. Sharma (Eds.). Woodhead Publishing, Cambridge, UK. pp. 393–431.

Cui, Z., L. Tu, M. Xu, Z. Chen, and C. Wang. 2020. The evaluation of dowel-bearing properties of laminated bamboo parallel to grain. *Structures* 25:956–964.

Deng, J., F. Chen, G. Wang, and W. Zhang. 2016. Variation of parallel-to-grain compression and shearing properties in moso bamboo culm (*Phyllostachys pubescens*). *BioResources* 11:1784–1795.

EN 1995-1-1. 2004. Eurocode 5: Design of timber structures—Part 1-1: General—Common rules and rules for buildings. European Union Per Regulation 305/2011, Directive 98/34/EC, Directive 2004/18/EC. 71 pp.

Eratodi, I. G. L. B., A. Triwiyono, A. Awaludin, and T. A. Prayitno. 2012. The effect of specific gravity on embedding strength of glued-laminated (glulam) bamboo: Numerical analysis and experiment. *ASEAN Eng. J. Part C* 3:30–40.

Gatoo, A., B. Sharma, M. Bock, H. Mulligan, and M. H. Ramage. 2014. Sustainable structures: Bamboo standards and building codes. *Proc. Inst. Civil Eng*. 167:189–196.

Gauss, C., J. H. Savastano, and K. A. Harries. 2019. Use of ISO 22157 mechanical test methods and the characterisation of Brazilian P. *edulis* bamboo. *Construction Building Mater*. 228:1–11.

Ghavami, K. 2016. Introduction to nonconventional materials and an historic retrospective of the field. *In:* Nonconventional and Vernacular Construction Materials. K. A. Harries and B. Sharma (Eds.). Woodhead Publishing, Cambridge, UK. pp. 37–61.

Hong, C., H. Li, R. Lorenzo, G. Wu, I. Corbi, O. Corbi, Z. Xiong, D. Yang. and H. Zhang. 2019. Review on connections for original bamboo structures. *J. Renewable Mater*. 7:713–730.

Hong, C., H. Li, Z. Xiong, R. Lorenzo, I. Corbi, O. Corbi, D. Wei, C. Yuan, D. Yang, and H. Zhang. 2020. Review of connections for engineered bamboo structures. *J. Building Eng*. 30:1–14.

Hu, W. and J. Zhang. 2020. Bolt-bearing yield strength of three-layered cross-laminated timber treated with phenol formaldehyde resin. *Forests* 11:1–12.

Huang, Y. S., F. L. Hsu, C. M. Lee, and J. Y. Juang. 2017. Failure mechanism of hollow tree trunks due to cross-sectional flattening. *R. Soc. Open Sci*. 4:1–10.

Janssen, J. J. A. 2000. Designing and building with bamboo. International Network for Bamboo and Rattan (INBAR) Technical Report 20. INBAR, Beijing, China. pp. 1–211.

Kappel, R., C. Mattheck, K. Bethge, and I. Tesari. 2004. Bamboo as a composite structure and its mechanical failure behaviour. *In:* Design and Nature II. Collins M. W. and C. A. Brebbia (Eds.). WIT Press, Ashurst, UK. pp. 285–293.

Keogh, L., P. O'Hanlon, P. O'Reilly, and D. Taylor. 2015. Fatigue in bamboo. *Int. J. Fatigue* 75:51–56.

Li, X., Q. Mou, H. Ren, X. Li, and Y. Zhong. 2020. Effects of moisture content and load orientation on dowel-bearing behavior of bamboo scrimber. *Construction Building Mater*. 262:1–10.

Liese, W. 1987. Research on bamboo. *Wood Sci. Technol*. 21:189–209.

Mottram, J. T. and G. J. Turvey (Eds.). 1998. EUR 18172, COST C1—State-of-the-Art Review on Design, Testing, Analysis and Applications of Polymeric Composite Connections. European Commission, Luxembourg.

Olmedo, A. and C. Santiuste. 2012. On the prediction of bolted single-lap composite joints. *Compos. Struct*. 94:2110–2117.

Paraskeva, T. S., G. Grigoropoulos, and E. G. Dimitrakopoulos. 2017. Design and experimental verification of easily constructible bamboo footbridges for rural areas. *Eng. Struct*. 143:540–548.

Ramful, R. 2018. Evaluation of the mechanical properties of bambusa bamboo culms with metallic joints through destructive testing. *J. Green Building* 13:1–19.

Ramful, R. and A. Sakuma. 2020. Investigation of the effect of inhomogeneous material on the fracture mechanisms of bamboo by finite element method. *Materials* 13:1–15.

Reynolds, T., B. Sharma, K. Harries, and M. Ramage. 2016. Dowelled structural connections in laminated bamboo and timber. *Compos Part B* 90:232–240.

Sawata, K. and M. Yasumura. 2002. Determination of embedding strength of wood for dowel-type fasteners. *J. Wood Sci*. 48:138–146.

Sotayo, A., D. Bradley, M. Bather, P. Sareh, M. Oudjene, I. El-Houjeyri, A. M. Harte, S. Mehra, C. O'Ceallaigh, P. Haller, S. Namari, A. Makradi, S. Belouettar, L. Bouhala, F. Deneufbourg, and Z. Guan. 2020. Review of state of the art of dowel laminated timber members and densified wood materials as sustainable engineered wood products for construction and building applications. *Dev. Built Environ*. 1:1–11.

Spatz, H. C. and K. J. Niklas. 2013. Modes of failure in tubular plant organs. *Am. J. Bot*. 100:332–336.

Trujillo, D., S. Jangra, and J. M. Gibson. 2017. Flexural properties as a basis for bamboo strength grading. *Proc. Inst. Civil Eng*. 170:284–294.

Trujillo, D. and L. F. Lopez. 2016. Bamboo material characterisation. *In:* Nonconventional and Vernacular Construction Materials. K. A. Harries and B. Sharma (Eds.). Woodhead Publishing, Cambridge, UK. pp. 365–392.

Wang, F. and J. Yang. 2020. Experimental and numerical investigations on load-carrying capacity of dowel-type bolted bamboo joints. *Eng. Struct*. 209:1–12.

Yang, L., X. Liu, Z. Jiang, G. Tian, S. Yang, and L. Shang. 2020. Compressive strength parallel to the grain in relation to moisture content in *Calamus simplicifolius* cane. *Forest Prod. J*. 70:309–316.

Zhang, X., J. Li, Z. Yu, Y. Yu, and H. Wang. 2017. Compressive failure mechanism and buckling analysis of the graded hierarchical bamboo structure. *J. Mater. Sci*. 52:6999–7007.

Zhou, J., D. Huang, Y. Song, and C. Ni. 2018. Experimental investigation on embedding strength perpendicular to grain of parallel strand bamboo. *Adv. Mater. Sci. Eng*. 2018:1–8.